Bioinorganic Chemistry Hot Paper

How to cite: Angew. Chem. Int. Ed. 2022, 61, e202208143
International Edition: doi.org/10.1002/anie.202208143
German Edition: doi.org/10.1002/ange.202208143

# Crucial Roles of a Pendant Imidazole Ligand of a Cobalt Porphyrin Complex in the Stoichiometric and Catalytic Reduction of Dioxygen

*Jindou Yang+, Ping Li+, Xialiang Li+, Lisi Xie, Ni Wang, Haitao Lei, Chaochao Zhang, Wei Zhang, Yong-Min Lee, Weiqiang Zhang,* Rui Cao,* Shunichi Fukuzumi,* and Wonwoo Nam**

**Abstract:** A cobalt porphyrin complex with a pendant imidazole base ($[(L_1)Co^{II}]$) is an efficient catalyst for the homogeneous catalytic two-electron reduction of dioxygen by 1,1′-dimethylferrocene ($Me_2Fc$) in the presence of triflic acid (HOTf), as compared with a cobalt porphyrin complex without a pendant imidazole base ($[(L_2)Co^{II}]$). The pendant imidazole ligand plays a crucial role not only to provide an imidazolinium proton for proton-coupled electron transfer (PCET) from $[(L_1)Co^{II}]$ to $O_2$ in the presence of HOTf but also to facilitate electron transfer (ET) from $[(L_1)Co^{II}]$ to $O_2$ in the absence of HOTf. The kinetics analysis and the detection of intermediates in the stoichiometric and catalytic reduction of $O_2$ have provided clues to clarify the crucial roles of the pendant imidazole ligand of $[(L_1)Co^{II}]$ for the first time.

## Introduction

The four-electron reduction of dioxygen ($O_2$) to water has merited special attention from the point of energy conversion, since it is the cathodic reaction in many types of fuel cells and the reduction process in aerobic respiration.[1–4] The two-electron reduction of $O_2$ to hydrogen peroxide ($H_2O_2$) has also attracted increasing interest recently, since $H_2O_2$ is used as a green oxidant and also utilized as a liquid solar fuel in $H_2O_2$ fuel cells.[5–9] Tremendous efforts have so far been devoted to clarifying the catalytic mechanisms of two-electron and four-electron reduction of $O_2$.[10–17] In the past decades, a variety of molecular complexes of the first-row transition metal elements, including Mn,[18] Fe,[19] Co,[20] Ni,[21] and Cu,[22,23] have been reported to be active catalysts for oxygen reduction reactions (ORR). The catalytic mechanisms of ORR with metal complexes have yet to be well understood because of the lack of detection of intermediates in relation with kinetics. Regarding the $O_2$ binding, an axial basic ligand is known to facilitate the $O_2$ binding to metal complexes.[24] However, the lack of information on the effect of a pendant axial base of metal complexes in homogeneous molecular catalysis of ORR has so far precluded to clarify the molecular mechanism of the crucial roles of pedant axial bases. On the other hand, a protonated base can act as a proton source for proton-coupled electron-transfer (PCET) reactions. If an axial basic ligand is attached to a metal complex, the $O_2$ binding in the absence and presence of proton is expected to be enhanced. Understanding the molecular mechanism of the effects of such a pendant axial base on ORR is indispensable to develop efficient molecular ORR catalysts. However, the lack of information on the effect of a pendant axial base of metal complexes in homogeneous molecular catalysis of ORR has so far precluded to clarify the molecular mechanism of the crucial roles of pedant axial bases.[25]

We report herein the synthesis and reactivity studies of a cobalt porphyrin complex with a pendant imidazole ligand, $[(L_1)Co^{II}]$, and a cobalt porphyrin without the pendant imidazole ligand, $[(L_2)Co^{II}]$ (Figure 1). Crucial roles of the pendant base in the stoichiometric and catalytic reduction of $O_2$ are demonstrated by comparing the reactivity of

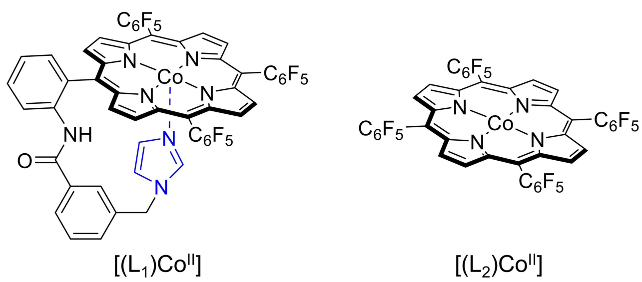


*Figure 1.* Chemical structures of a cobalt porphyrin with a pendant imidazole base, $[(L_1)Co^{II}]$, and a reference cobalt porphyrin without the pendant imidazole base, $[(L_2)Co^{II}]$.

[*] J. Yang,+ Prof. Dr. Y.-M. Lee, Prof. Dr. S. Fukuzumi, Prof. Dr. W. Nam
Department of Chemistry and Nano Science
Ewha Womans University
Seoul 03760 (Korea)
E-mail: fukuzumi@chem.eng.osaka-u.ac.jp
wwnam@ewha.ac.kr

P. Li,+ Dr. X. Li,+ Dr. L. Xie, Dr. N. Wang, Dr. H. Lei, C. Zhang, Prof. Dr. W. Zhang, Prof. Dr. W. Zhang, Prof. Dr. R. Cao
Key Laboratory of Applied Surface and Colloid Chemistry, Xi'an Key Laboratory of Organometallic Material Chemistry, School of Chemistry and Chemical Engineering, Shaanxi Normal University
Xi'an 710119 (China)
E-mail: zwq@snnu.edu.cn
ruicao@snnu.edu.cn

[+] These authors contributed equally to this work.

 

$[(L_1)Co^{II}]$ and $[(L_2)Co^{II}]$ in those $O_2$ reduction reactions. The catalytic mechanism of two-electron/two-proton reduction of $O_2$ with $[(L_1)Co^{II}]$ and $[(L_2)Co^{II}]$ in the presence of triflic acid (HOTf) is clarified based on the kinetic analysis together with the detection of intermediate(s) by electron paramagnetic resonance (EPR) spectroscopy. PECT from $[(L_1)Co^{II}]$ and $[(L_2)Co^{II}]$ to $O_2$ is shown to be the rate-determining step (r.d.s.) in the two-electron/two-proton reduction of $O_2$ by 1,1′-dimethylferrocene ($Me_2Fc$) with $[(L_1)Co^{II}]$ and $[(L_2)Co^{II}]$, when the pendant imidazole ligand of $[(L_1)Co^{II}]$ plays a crucial role to facilitate the PCET process. To the best of our knowledge, this is the first time to clarify the crucial roles of a pendant basic ligand in both ET and PCET processes in ORR by metalloporphyrins.

## Results and Discussion

### Characterization of $[(L_1)Co^{II}]$

$[(L_1)Co^{II}]$ was synthesized according to the procedures presented in Scheme S1 (synthetic and characterization details are described in Supporting Information, Figures S1–S6). The identity and purity of $[(L_1)Co^{II}]$ were confirmed by the cold-spray ionization time-of-flight mass spectrometry (CSI-MS) and elemental analysis. In the CSI-MS spectrum of an MeCN solution of $[(L_1)Co^{II}]$, an ion peak at mass-to-charge ratio ($m/z$) of 1181.2 was assigned as $[(L_1)Co^{II}(MeCN)]^+$ (calcd. $m/z$ of 1181.1) (Figure S6). The cyclic voltammogram (CV) of $[(L_1)Co^{II}]$ in tetrahydrofuran (THF) at a glassy carbon electrode displayed two quasi-reversible reduction waves at $E_{1/2}$ vs ferrocene/ferrocenium ($Fc/Fc^+$) $= -1.41$ and $-2.10$ V and one irreversible oxidation wave at $E_{p,a}$ vs. $Fc/Fc^+ = -0.21$ V (Figure S7). The two reduction waves can be assigned to the formal $Co^{II/I}$ and $Co^{I/0}$ couples,[26] whereas the oxidation wave is assigned to the formal $Co^{III/II}$ process. As a control, we synthesized a Co tetra(pentafluorophenyl)porphyrin complex ($[(L_2)Co^{II}]$), which is an imidazole-free analogue of $[(L_1)Co^{II}]$. The CV of $[(L_2)Co^{II}]$ showed two quasi-reversible reduction waves at $E_{1/2} = -0.87$ and $-1.80$ V vs. $Fc/Fc^+$ and one irreversible oxidation wave at $E_{p,a} = 0.58$ V vs. $Fc/Fc^+$ (Figure S8). As compared to $[(L_2)Co^{II}]$ (Figure S8), the redox couples of $[(L_1)Co^{II}]$ show a large cathodic (negative) shift by more than 0.50 V, because of the binding of the tethered electron-donating imidazole ligand at the axial position of Co ion in $[(L_1)Co^{II}]$ (Figure S7). The anodic shift may also result from the difference between the $C_6F_5$ (in $L_2$) and the amidophenyl (in $L_1$) groups. $[(L_1)Co^{II}]$ and $[(L_2)Co^{II}]$ displayed slightly different EPR spectra under $N_2$ with EPR parameters of $g_x = 2.306$, $g_y = 2.306$, $g_z = 2.036$; $A_x = 0.80$, $A_y = 0.80$, $A_z = 7.68$ mT for $[(L_1)Co^{II}]$ (Figure 2a) and those of $g_x = 2.304$, $g_y = 2.304$, $g_z = 2.030$; $A_x = 0.80$, $A_y = 0.80$, $A_z = 9.95$ mT for $[(L_2)Co^{II}]$ (Figure S9a), indicating different coordination structures of their Co ions. In $[(L_1)Co^{II}]$ and $[(L_2)Co^{II}]$, the $d^7$ $Co^{II}$ ion is incorporated at the center of porphyrin macrocycles through four N atoms, which define an equatorial plane.[25,27,28] In the structure of $[(L_1)Co^{II}]$, one axial position of Co is occupied by an imidazole group, leading to a five-coordinate square pyramid geometry. However, in the structure of $[(L_2)Co^{II}]$, the $Co^{II}$ ion has a four-coordinate square planar geometry.

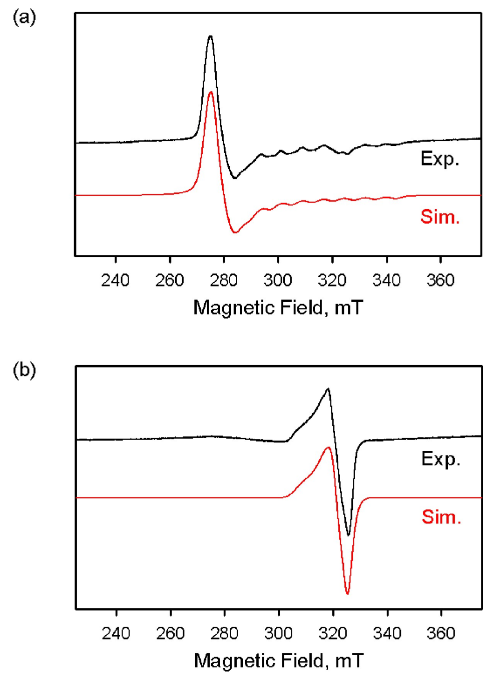


*Figure 2.* a) Experimental (black line) and simulated (red line) X-band EPR spectra of $[(L_1)Co^{II}]$ (0.20 mM) recorded in deaerated MeCN at 80 K. Simulation parameters for the $S = 1/2$ $Co^{II}$ ground state: $g = [2.306, 2.306, 2.036]$ and $A = [0.80, 0.80, 7.68]$ mT. b) Experimental (black line) and simulated (red line) X-band EPR spectra of $[(L_1)Co^{III}(O_2^{\bullet-})]$ (0.20 mM) recorded in $O_2$-saturated MeCN at 80 K. Simulation parameters for the $S = 1/2$ $[(L_1)Co^{III}(O_2^{\bullet-})]$ ground state: $g = [2.062, 2.000, 1.997]$ and $A = [1.8, 1.1, 0.6]$ mT.

### Binding of $O_2$

When $O_2$ was introduced into a deaerated MeCN solution of $[(L_1)Co^{II}]$ at 298 K, the absorbance at 407 nm due to $[(L_1)Co^{II}]$ decreased with increasing concentration of $O_2$, accompanied by an increase in absorbance at 428 nm (Figure 3a). When an EPR spectrum of an $O_2$-saturated solution of $[(L_1)Co^{II}]$ was measured at 80 K, the EPR spectrum of $[(L_1)Co^{II}]$ was changed to that with $g_z = 2.062$, $g_x = 2.000$, $g_y = 1.997$; $A_z = 1.8$, $A_x = 1.1$, $A_y = 0.6$ mT, which is assigned to the $Co^{III}$-superoxide porphyrin ($[(L_1)Co^{III}(O_2^{\bullet-})]$), as shown in Figure 2b, by comparing with the EPR parameters of the reported $Co^{III}$-superoxide porphyrin ($g_z = 2.074$, $g_x = 2.001$, $g_y = 2.001$; $A_z = 1.64$, $A_x = 1.03$, $A_y = 1.03$ mT).[29] Thus, the absorption band at 428 nm is assigned to $[(L_1)Co^{III}(O_2^{\bullet-})]$. In such a case, the equilibrium constant ($K$) of binding of $O_2$ to $[(L_1)Co^{II}]$ to produce $[(L_1)Co^{III}(O_2^{\bullet-})]$ is determined using Equation (1),

$$(\alpha - 1)^{-1} = K[O_2] \tag{1}$$

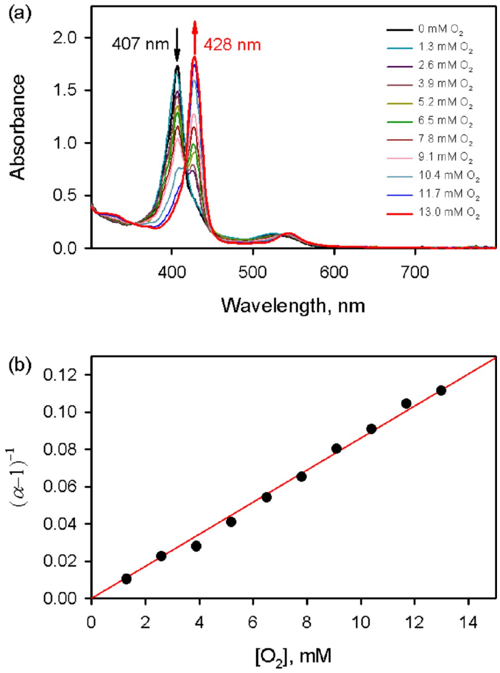


*Figure 3.* a) UV/Visible absorption spectral change of $[(L_1)Co^{II}]$ (10 μM, black line) in $O_2$ binding in the presence of various concentrations of $O_2$ in MeCN at 298 K. b) Plot of $(\alpha-1)^{-1}$ vs concentration of $O_2$ to determine the equilibrium constant ($K$), where $\alpha=[Co^{II}]_0/[Co^{III}]$ and $[Co^{III}]=(A-A_0)/(\varepsilon_{Co^{III}}-\varepsilon_{Co^{II}})$ at 428 nm.

where $\alpha=[Co^{II}]_0/[Co^{III}]$, $[Co^{III}]=(A-A_0)/(\varepsilon_{Co^{III}}-\varepsilon_{Co^{II}})$ and $A$ and $A_0$ are absorbances at 428 nm due to $[(L_1)Co^{III}(O_2^{\bullet-})]$ and $[(L_1)Co^{II}]$, respectively. From the slope of a linear plot of $(\alpha-1)^{-1}$ vs. $[O_2]$ in Figure 3b, the $K$ value is determined to be 9.0 $M^{-1}$ at 298 K. A linear correlation in Figure 3b suggests that formation of dinuclear cobalt(III)-peroxo species is not involved in the reaction of $[(L_1)Co^{II}]$ and $O_2$.

When $[(L_1)Co^{II}]$ was replaced by $[(L_2)Co^{II}]$ that has no pendant imidazole base, the reaction of $[(L_2)Co^{II}]$ with $O_2$ has hardly occurred in $O_2$-saturated MeCN at 298 K (Scheme 1). When the temperature was lowered to 233 K, the formation of $[(L_2)Co^{III}(O_2^{\bullet-})]$ was observed by EPR spectroscopy (Figure S9b and S10).

### *Acid-Promoted Reduction of $O_2$ by $[(L_1)Co^{II}]$ and $[(L_2)Co^{II}]$*

When HOTf (4.0 mM) was added to an aerated MeCN solution of $[(L_1)Co^{II}]$ (0.20 mM), the absorption band at 407 nm due to $[(L_1)Co^{II}]$ disappeared, accompanied by an increase in absorbance at 430 nm (Figure S11a). The EPR of the resulting solution gave no signal (Figure S12). Thus, this observation indicates that $[(L_1)Co^{II}]$ was oxidized by $O_2$ to $[(L_1H)Co^{III}]^{2+}$ in the presence of HOTf via PCET. The rate of the decrease of the absorbance at 407 nm due to $[(L_1)Co^{II}]$, as well as the increase in absorbance at 430 nm due to $[(L_1H)Co^{III}]^{2+}$, in the reaction of $[(L_1)Co^{II}]$ with $O_2$ in the presence of HOTf obeyed the first-order kinetics with respect to the concentration of HOTf (see Figures S13 and S14). The observed first-order rate constant ($k_{obs1}$) increased

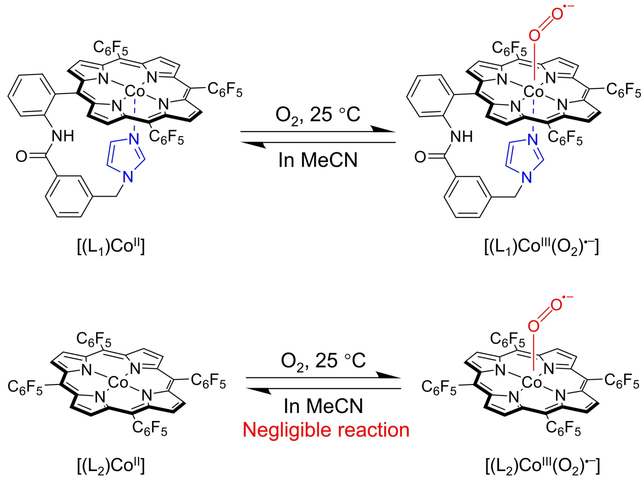


*Scheme 1.* Electron-transfer equilibria of $[(L_1)Co^{II}]$ and $[(L_2)Co^{II}]$ with $O_2$.

linearly with increasing the concentration of $O_2$ (black circles in Figure 4). The $k_{obs1}$ value in the reaction of $[(L_1)Co^{II}]$ with $O_2$ in the presence of HOTf also increased with increasing concentration of HOTf, as shown in Figure 5a. Since HOTf first binds to the imidazole base that is the much more basic than the amide part, the linear correlation between $k_{obs1}$ vs [HOTf] suggests that another HOTf molecule is required for the reaction of $[(L_1)Co^{II}]$ with $O_2$. It should be mentioned that two HOTf molecules or Lewis acidic molecules are required for acid-promoted electron transfer (APET) from electron donors to a $Cr^{III}$-superoxide complex.[30,31] Thus, the rate of the disappearance of $[(L_1)Co^{II}]$ in the acid-promoted two-electron reduction of $O_2$ by two equivalents of $Co_1^{II}$ ($[(L_1)Co^{II}]$) and $H^+$ is given by Equation (2),

$$d[Co_1^{II}]/dt = -k_{3rd}[Co_1^{II}][O_2][H^+] \quad (2)$$

where $k_{3rd}$ is the observed third-order rate constant. The observed kinetics in Equation (2) can be well explained by the mechanism of the acid-promoted two-electron reduction of $O_2$ by $Co_1^{II}$ with $H^+$ as shown in Scheme 2a, where the

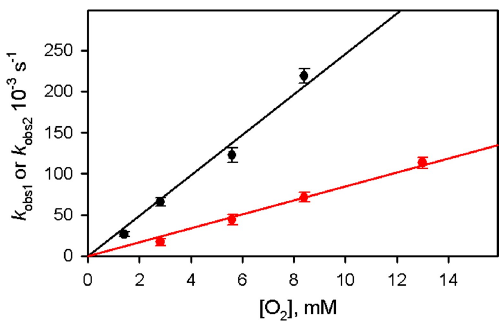


*Figure 4.* Plots of the first-order rate constant of the reaction of $[(L_1)Co^{II}]$ (10 μM, black circles) and $[(L_2)Co^{II}]$ (10 μM, red circles) in the presence of $O_2$ and HOTf (4.0 mM) vs. concentration of $O_2$ in MeCN at 298 K.

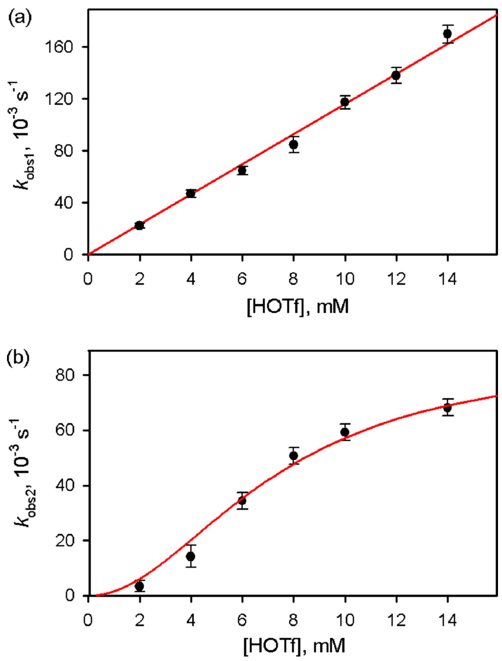


***Figure 5.*** Plots of the first-order rate constant in the reaction of a) $[(L_1)Co^{II}]$ (10 μM) and b) $[(L_2)Co^{II}]$ (10 μM) with $O_2$ (2.8 mM) in the presence of HOTf in aerated MeCN at 298 K vs. concentration of HOTf.

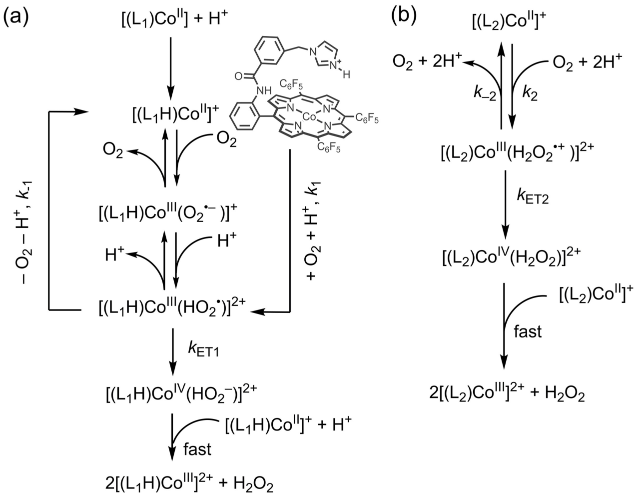

***Scheme 2.*** Mechanism of acid-promoted two-electron/two-proton reduction of $O_2$ by a) $[(L_1)Co^{II}]$ with a pendant base and b) $[(L_2)Co^{II}]$ without a pendant base.

pendant base of $[(L_1)Co^{II}]$ is protonated by HOTf to produce $[(L_1H)Co^{II}]^+$. Then, APET from $[(L_1H)Co^{II}]^+$ to $O_2$ with one equivalent of $H^+$ occurs to produce $[(L_1H)Co^{III}(HO_2^\bullet)]^{2+}$, in which $HO_2^\bullet$ may be hydrogen-bonded to the protonated base. In competition with the back electron transfer to regenerate $[(L_1H)Co^{II}]^+$, the intramolecular electron transfer from the $Co^{III}$ center to the $HO_2^\bullet$ moiety occurs to produce $[(L_1H)Co^{IV}(HO_2^-)]^{2+}$, followed by rapid electron transfer from $[(L_1H)Co^{II}]^+$ to $[(L_1H)Co^{IV}(HO_2^-)]^{2+}$ with $H^+$ to yield two equivalents of $[(L_1H)Co^{III}]^{2+}$ and one equivalent of $H_2O_2$ (Scheme 2a). $[(L_1H)Co^{III}(HO_2^\bullet)]^{2+}$ could be detected by EPR as shown in Figure S15a (also see Figure S16 and S17). Unfortunately, we could not distinguish the absorption spectra due to $[(L_1H)Co^{III}(HO_2^\bullet)]^{2+}$ and $[(L_1H)Co^{III}]^{2+}$.

According to Scheme 2a, the rate of the disappearance of $[(L_1H)Co^{II}]^+$ is given by Equation (3)

$$\mathrm{d}[Co_1^{II}]/\mathrm{d}t = -k_1[Co_1^{II}][O_2][H^+] + k_{-1}[Co_1^{III}(HO_2^\bullet)] - k_{ET1}[Co_1^{III}(HO_2^\bullet)] \quad (3)$$

where $Co_1^{III}(HO_2^\bullet)$ denotes $[(L_1H)Co^{III}(HO_2^\bullet)]^{2+}$. The rate constants of $k_1$, $k_{-1}$ and $k_{ET1}$ are those of APET from $[(L_1H)Co^{II}]^+$ to $O_2$ with $H^+$, back electron transfer to regenerate $[(L_1H)Co^{II}]^+$ and intramolecular electron transfer from the $Co^{III}$ center to the $HO_2^\bullet$ moiety to produce $[(L_1H)Co^{IV}(HO_2^-)]^{2+}$, respectively. On the other hand, the rise and decay of $[(L_1H)Co^{III}(HO_2^\bullet)]^{2+}$ is given by Equation (4).

$$\mathrm{d}[Co_1^{III}(HO_2^\bullet)]/\mathrm{d}t = k_1[Co_1^{II}][O_2][H^+] - k_{-1}[Co_1^{III}(HO_2^\bullet)] - k_{ET1}[Co_1^{III}(HO_2^\bullet)] \quad (4)$$

By summing Equations (3) and (4), Equation (5) is derived. Applying the steady-state approximation, Equation (6) is obtained from Equation (4) when $\mathrm{d}[Co_1^{III}(HO_2^\bullet)]/\mathrm{d}t = 0$.

$$\mathrm{d}([Co_1^{II}] + [Co_1^{III}(HO_2^\bullet)])/\mathrm{d}t = -2k_{ET1}[Co_1^{III}(HO_2^\bullet)] \quad (5)$$

$$[Co_1^{III}(HO_2^\bullet)] = k_1[Co_1^{II}][O_2][H^+]/(k_{-1} + k_{ET1}) \quad (6)$$

From Equations (5) and (6), Equation (7) is derived under the conditions such that $k_{ET1} \ll k_{-1}$ (see Supporting Information for the derivation). Equation (7) derived from Scheme 2a agrees with the observed kinetics in Equation (2) (Figure 5a), where $k_{obs1} = 2k_{ET1}K_1$ ($K_1 = k_1/k_{-1}$). Under the conditions of Figure 5a, $K_1[O_2][H^+] \ll 1$.

$$\mathrm{d}[Co_1^{II}]/\mathrm{d}t = -2k_{ET1}K_1[Co_1^{II}][O_2][H^+]/(1 + K_1[O_2][H^+]) \quad (7)$$

The decay rate of absorbance at 405 nm due to $[(L_2)Co^{II}]$ as well as the rate of increase in absorbance at 428 nm due to the reaction of $[(L_2)Co^{II}]$ with $O_2$ and HOTf also obeyed the first-order kinetics (Figures S11b, S19 and S20). The observed first-order rate constant increased linearly with increasing concentration of $O_2$ (red circles in Figure 4). The $k_{obs2}$ value in the reaction of $[(L_2)Co^{II}]$ with $O_2$ and HOTf also increased with increasing concentration of HOTf, but it exhibited a sigmoidal dependence on [HOTf], as shown in Figure 5b. In the case of $[(L_2)Co^{II}]$ without a pendant base, two protons are required to promote PCET from $[(L_2)Co^{II}]$ to $O_2$, as shown in Scheme 2b. According to Scheme 2b, the rate of disappearance of $Co_2^{II}$ $[(L_2H)Co^{II}]$ is given by Equation (8), where $Co_2^{III}(H_2O_2^{\bullet+})$ denotes $[(L_2)Co^{III}(H_2O_2^{\bullet+})]^{2+}$.

$$\mathrm{d}[\mathrm{Co_2}^{\mathrm{II}}]/\mathrm{d}t = -k_2[\mathrm{Co_2}^{\mathrm{II}}][\mathrm{O_2}][\mathrm{H^+}]^2 + k_{-2}[\mathrm{Co_2}^{\mathrm{III}}(\mathrm{H_2O_2}^{\bullet+})] - k_{\mathrm{ET2}}[\mathrm{Co_2}^{\mathrm{III}}(\mathrm{H_2O_2}^{\bullet+})] \quad (8)$$

The rate constants of $k_2$, $k_{-2}$ and $k_{\mathrm{ET2}}$ are those of APET from $[(L_2)Co^{II}]^+$ to $O_2$ in the presence of $H^+$, back electron transfer to regenerate $[(L_2)Co^{II}]^+$ and intramolecular electron transfer from the $Co^{III}$ center to the $H_2O_2^{\bullet+}$ moiety to produce $[(L_2)Co^{IV}(H_2O_2)]^{2+}$, respectively, which maybe is similar to the acid-promoted ET reduction of a $Cr^{III}$-superoxo complex occurring via the $Cr^{III}(H_2O_2^{\bullet+})$ complex in which $H_2O_2^{\bullet+}$ can coordinate to the $Cr^{III}$ center.[31] The EPR of $[(L_2H)Co^{III}(HO_2^{\bullet})]^{2+}$ was observed as shown in Figure S15b (also see Figure S16 and S18). The change in the $g$ values results from the spin-orbit interaction with the split $\pi_g$ levels due to the protonation of $[(L_1)Co^{III}(O_2^{\bullet-})]$ and $[(L_2)Co^{III}(O_2^{\bullet-})]$.[32] On the other hand, the rise and decay of $[(L_2)Co^{III}(H_2O_2^{\bullet+})]^{2+}$ is given by Equation (9). By summing Equations (8) and (9), Equation (10) is derived.

$$\mathrm{d}[\mathrm{Co_2}^{\mathrm{III}}(\mathrm{H_2O_2}^{\bullet+})]/\mathrm{d}t = k_2[\mathrm{Co_2}^{\mathrm{II}}][\mathrm{O_2}][\mathrm{H^+}]^2 - k_{-2}[\mathrm{Co_2}^{\mathrm{III}}(\mathrm{H_2O_2}^{\bullet+})] - k_{\mathrm{ET1}}[\mathrm{Co_2}^{\mathrm{III}}(\mathrm{H_2O_2}^{\bullet})] \quad (9)$$

$$\mathrm{d}([\mathrm{Co_2}^{\mathrm{II}}] + [\mathrm{Co_2}^{\mathrm{III}}(\mathrm{H_2O_2}^{\bullet+})])/\mathrm{d}t = -2k_{\mathrm{ET2}}[\mathrm{Co_2}^{\mathrm{III}}(\mathrm{H_2O_2}^{\bullet+})] \quad (10)$$

Applying the steady-state approximation, Equation (11) is obtained from Equation (9) when $\mathrm{d}[\mathrm{Co_2}^{\mathrm{III}}(\mathrm{H_2O_2}^{\bullet+})]/\mathrm{d}t = 0$. From Equations (10) and (11), Equation (12) is derived under the conditions such that $k_{\mathrm{ET2}} \ll k_{<M->2}$ (see Supporting Information for the derivation). Equation (12) derived from Scheme 2b agrees with the observed kinetics in Figure 5b, where $k_{\mathrm{obs2}} = 2k_{\mathrm{ET2}}K_2$ ($K_2 = k_2/k_{-2}$).

$$[\mathrm{Co_2}^{\mathrm{III}}(\mathrm{H_2O_2}^{\bullet+})] = k_2[\mathrm{Co_2}^{\mathrm{II}}][\mathrm{O_2}][\mathrm{H^+}]^2/(k_{-2} + k_{\mathrm{ET2}}) \quad (11)$$

$$\mathrm{d}[\mathrm{Co_2}^{\mathrm{II}}]/\mathrm{d}t = -2k_{\mathrm{ET2}}K_2[\mathrm{Co_2}^{\mathrm{II}}][\mathrm{O_2}][\mathrm{H^+}]^2/(1 + K_2[\mathrm{O_2}][\mathrm{H^+}]^2) \quad (12)$$

The observed first-order rate constant $k_{\mathrm{obs2}}$ (also see Figure S20) in Equation (12) is rewritten by Equation (13). A linear plot of $k_{\mathrm{obs2}}^{-1}$ vs $[\mathrm{HOTf}]^{-2}$ is obtained, as shown in Figure S21, indicating the validity of Scheme 2b. From the intercept and slope, the $2k_{\mathrm{ET2}}$ and $K_2$ values were determined to be $(9.1 \pm 1.6) \times 10^{-2}\ \mathrm{s^{-1}}$ and $(1.8 \pm 0.4) \times 10^4\ \mathrm{M^{-2}}$, respectively.

$$(k_{\mathrm{obs2}})^{-1} = (2k_{\mathrm{ET2}}K_2[\mathrm{O_2}][\mathrm{HOTf}]^2)^{-1} + (2k_{\mathrm{ET2}})^{-1} \quad (13)$$

The linear dependence of $k_{\mathrm{obs1}}$ of $[(L_1)Co^{II}]$ with $O_2$ and HOTf on [HOTf] in Figure 5a indicates that the $O_2^{\bullet-}$ moiety in $[(L_1H)Co^{III}(O_2^{\bullet-})]^+$ is readily protonated by the protonated pendant base and $K_1$ corresponds to the second protonation to produce $[(L_1H)Co^{III}(HO_2^{\bullet})]^{2+}$, followed by the rate-determining intramolecular electron transfer from the $Co^{III}$ moiety to the $HO_2^{\bullet}$ moiety of $[(L_1H)Co^{III}(HO_2^{\bullet})]^{2+}$ to produce $[(L_1H)Co^{IV}(HO_2^-)]^{2+}$, and the subsequent rapid electron transfer from $[(L_1H)Co^{II}]^+$ to $[(L_1H)Co^{IV}(HO_2^-)]^{2+}$ to produce two equivalents of $[(L_1H)Co^{III}]^{2+}$ and $H_2O_2$ (Scheme 2a). The $k_{\mathrm{obs1}}$ values are much larger than the $k_{\mathrm{obs2}}$ values in the HOTf concentration range from 4.0 to 14 mM (Figure 5). The maximum ratio of $k_{\mathrm{obs1}}/k_{\mathrm{obs2}}$ value is 5.2 at the concentration of 2.0 mM of HOTf. Such an enhanced reactivity of $[(L_1)Co^{II}]$ with a pendant imidazole base towards the PCET reaction with $O_2$, as compared with that without the pendant imidazole base $[(L_2)Co^{II}]$, may result from the first intramolecular protonation to $[(L_1H)Co^{III}(O_2^{\bullet-})]$ by the protonated pendant base with the much larger binding constant than the first intermolecular protonation to $[(L_2)Co^{III}(O_2^{\bullet-})]$. Thus, the pendant imidazole base plays an important role to enhance the proton-promoted electron-transfer reactivity of the $Co^{II}$ porphyrin complex towards $O_2$.

### *Catalytic Two-Electron/Two-Proton Reduction of $O_2$ by $[(L_1)Co^{II}]$ and 1,1′-Dimethylferrocene*

When 1,1′-dimethylferrocene ($Me_2Fc$) was employed as an electron donor, the two-electron/two-proton reduction of $O_2$ by $Me_2Fc$ with HOTf occurred in the presence of a catalytic amount of $[(L_1)Co^{II}]$ to produce $Me_2Fc^+$ and $H_2O_2$ [Eq. (14)]. It should be noted that no oxidation of $Me_2Fc$ by $O_2$ occurred in the absence of $[(L_1)Co^{II}]$ under otherwise the same reaction conditions. The stoichiometry of the catalytic oxygen reduction was confirmed under the reaction conditions using aerated $O_2$ (2.8 mM) in MeCN. The formation of $Me_2Fc^+$ (1.0 mM) in the reduction of $O_2$ was observed in the presence of a catalytic amount of $[(L_1)Co^{II}]$ (10 μM) with $Me_2Fc$ (1.0 mM) and HOTf (1.0 mM) in aerated MeCN (Figure S22). When a large excess of $Me_2Fc$ (10 mM) and HOTf (10 m M) were used in the reduction of $O_2$ (2.8 mM) in the presence of a catalytic amount of $[(L_1)Co^{II}]$ (10 μM), $Me_2Fc^+$ (5.6 mM) formed in the catalytic reduction of $O_2$ by $Me_2Fc$ at the end of the catalytic reaction is twice the concentration of $O_2$ (2.8 mM) in aerated MeCN (Figure S23). In this catalytic reaction, TON and TOF values were determined to be 800 at 6000 s and 2.0 $s^{-1}$, respectively. This result clearly indicates that the two-electron/two-proton reduction of $O_2$ occurred to produce 2 equiv of $Me_2Fc^+$ and there is no further reduction to produce more than 2 equiv of $Me_2Fc^+$. The stoichiometry of Equation (14) was confirmed, showing the 2:1 stoichiometry between $[Me_2Fc^+]$ and $[O_2]$ and the 1:1 stoichiometry between $[Me_2Fc^+]$ and [HOTf]. The formation of $H_2O_2$ was confirmed by the redox titrations (Figure S24).[33]

$$2\mathrm{Me_2Fc} + \mathrm{O_2} + 2\mathrm{H^+} \xrightarrow{[(\mathrm{L_1})\mathrm{Co^{II}}]} 2\mathrm{Me_2Fc^+} + \mathrm{H_2O_2} \quad (14)$$

The initial rate ($R_{\mathrm{init1}}$) of the formation of $Me_2Fc^+$ monitored at 650 nm due to $Me_2Fc^+$ in the catalytic two-electron/two-proton reduction of $O_2$ by $Me_2Fc$ with $[(L_1)Co^{II}]$ in the presence of HOTf [Eq. (14)] increased linearly with increasing concentration of $Me_2Fc$ (Figure S25). The overall rate of the formation of $Me_2Fc^+$ also obeyed the first-order kinetics (Figure S26). The observed first-order rate constant increased linearly with increasing the concentration of $[(L_1)Co^{II}]$ [Eq. (15), Figure S27].

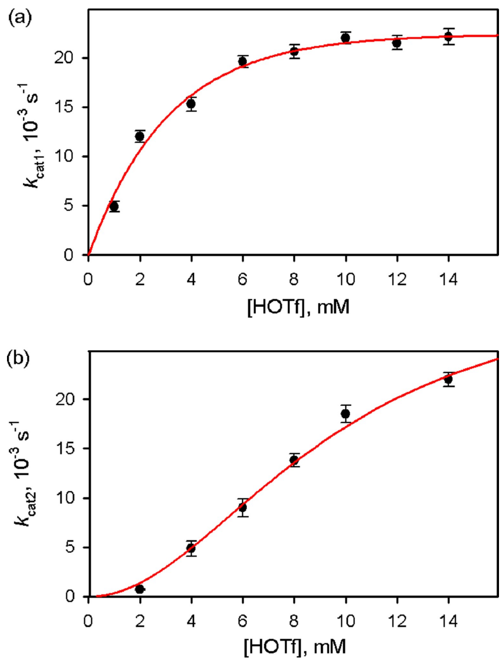


*Figure 6.* Plots of the first-order rate constant for the formation of $Me_2Fc^+$ in the catalytic reduction of $O_2$ (2.8 mM) by $Me_2Fc$ (1.0 mM) with HOTf in the presence of a catalytic amount of a) $[(L_1)Co^{II}]$ (10 μM) and b) $[(L_2)Co^{II}]$ (10 μM) in aerated MeCN at 298 K vs concentration of HOTf.

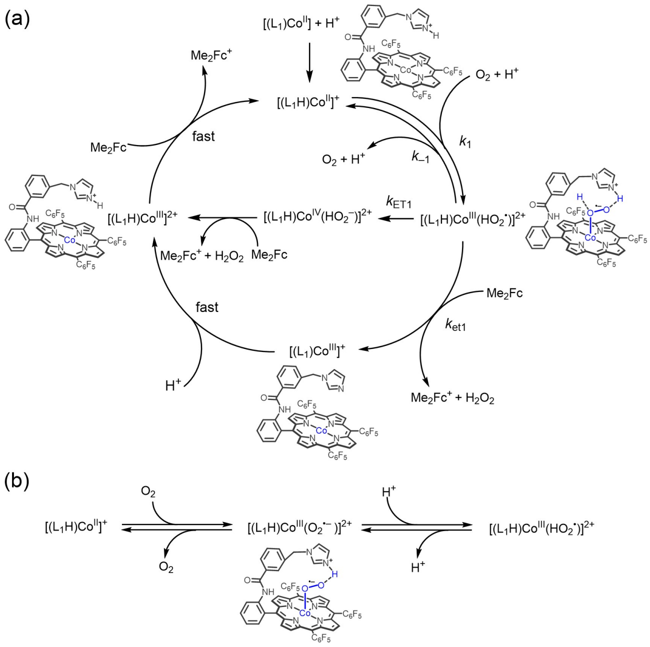


*Scheme 3.* Proposed mechanism of catalytic two-electron/two-proton reduction of $O_2$ by $Me_2Fc$ with $[(L_1)Co^{II}]$ in the presence of HOTf.

$$d[Me_2Fc^+]/dt = k_{cat1}[Me_2Fc][(L_1)Co^{II}] \quad (15)$$

The $k_{cat1}$ value at 1.0 mM of HOTf increased linearly with increasing the concentration of $O_2$ ($[O_2]$) (Figure S28a), whereas the $k_{cat1}$ value at 10 mM HOTf remained constant irrespective of $[O_2]$ (Figure S28b). In contrast to the case of Figure 5a, where $k_{obs1}$ of APET from $[(L_1H)Co^{II}]^+$ to $O_2$ was proportional to [HOTf], the $k_{cat1}$ value exhibits a saturated dependence on [HOTf] to reach a constant value, as shown in Figure 6a (see Figures S29 and S30) for the time dependence and the first-order plot, respectively). The reason of such a drastic change in the dependence of $k_{cat1}$ on $[O_2]$ depending on [HOTf] and the saturated dependence of $k_{cat1}$ on [HOTf] is discussed in relation with the catalytic mechanism (vide infra). The first-order kinetics with respect to $[Me_2Fc]$ in Equation (15) and the first-order dependence on $[O_2]$ (Figure S28a) suggest that electron transfer from $Me_2Fc$ to $[(L_1H)Co^{III}(HO_2^{\bullet})]^{2+}$ following PCET (or APET) from $[(L_1H)Co^{II}]^+$ to $O_2$ is much faster than the intramolecular electron transfer from the $Co^{III}$ center to the $HO_2^{\bullet}$ moiety in $[(L_1H)Co^{III}(HO_2^{\bullet})]^{2+}$, being the r.d.s. in the catalytic cycle shown in Scheme 3. Electron transfer from $Me_2Fc$ to $[(L_1H)Co^{III}]^{2+}$ produces another molecule of $Me_2Fc^+$, regenerating $[(L_1H)Co^{II}]^+$. The saturated dependence of $k_{cat1}$ on [HOTf] to reach a constant value in Figure 6a indicates that the r.d.s. is changed in the presence of a large amount of HOTf to be electron transfer from $Me_2Fc$ to $[(L_1H)Co^{III}]^{2+}$, when the $k_{cat1}$ value becomes independent of $[O_2]$ (Figure S28b).

### *Catalytic Two-Electron/Two-Proton Reduction of $O_2$ by $[(L_2)Co^{II}]$ and 1,1′-Dimethylferrocene*

The two-electron/two-proton reduction of $O_2$ by $Me_2Fc$ with HOTf also occurred in the presence of a catalytic amount of $[(L_2)Co^{II}]$ to produce $Me_2Fc^+$ and $H_2O_2$ [Eq. (14)], in which $[(L_1)Co^{II}]$ is replaced by $[(L_2)Co^{II}]$). The initial rate ($R_{init2}$) of the formation of $Me_2Fc^+$ monitored at 650 nm due to $Me_2Fc^+$ in the catalytic two-electron/two-proton reduction of $O_2$ by $Me_2Fc$ with $[(L_2)Co^{II}]$ in the presence of HOTf [Eq. (14)] increased linearly with increasing concentration of $Me_2Fc$ (Figure S31). The overall rate of the formation of $Me_2Fc^+$ also obeyed the first-order kinetics (Figure S32). The TON and TOF values, which was obtained in the catalytic two-electron reduction of $O_2$ (2.8 mM) by $Me_2Fc$ (2.0 mM) with $[(L_2)Co^{II}]$ (10 μM) in the presence of HOTf (10 mM) in aerated MeCN at 298 K, were determined to be 200 at 1000 s and 2.0 $s^{-1}$, respectively. The observed first-order rate constant, $k_{cat2}$, increased linearly with increasing concentration of $[(L_2)Co^{II}]$ as the case of $[(L_1)Co^{II}]$ (vide supra) (Figure S33). The $k_{cat2}$ value also increased linearly with increasing concentration of $[O_2]$ at 4.0 mM HOTf (Figure S34). The $k_{cat2}$ value increased with increasing concentration of HOTf to exhibit a sigmoidal dependence on [HOTf] to reach a constant value, as shown in Figure 6b (also see Figures S35 and S36), as the case of the reaction of $[(L_2)Co^{II}]$ with $O_2$ and HOTf.

These kinetic analyses lead us to propose a mechanism for the catalytic two electron reduction of $O_2$ by $Me_2Fc$ with HOTf in the presence of a catalytic amount of $[(L_2)Co^{II}]$, as shown in Scheme 4 (vide infra). The catalytic reaction is started by PCET (or APET) from $[(L_2)Co^{II}]$ to $O_2$ with two protons ($k_2$) to produce $[(L_2)Co^{III}(H_2O_2^{\bullet+})]^{2+}$, followed by electron transfer from $Me_2Fc$ to $[(L_2)Co^{III}(H_2O_2^{\bullet+})]^{2+}$ ($k_{et2}$) to produce $[(L_2)Co^{III}]^+$ and $H_2O_2$. Fast electron transfer from $Me_2Fc$ to $[(L_2)Co^{III}]^+$ occurred to produce $Me_2Fc^+$, accompanied by the regeneration of $[(L_2)Co^{II}]$ to complete the catalytic cycle. Because the catalytic rate of formation of $Me_2Fc^+$ obeys the first-order kinetics in terms of $[Me_2Fc]$, the rate-determining step is suggested to be electron transfer from $Me_2Fc$ to $[(L_2)Co^{III}(H_2O_2^{\bullet+})]^{2+}$ ($k_{et2}$) in Scheme 4, which is produced by the reaction of $[(L_2)Co^{II}]$ with $O_2$ and $2H^+$ ($k_2$), in competition with the back reaction ($k_{-2}$). This r.d.s. is followed by fast electron transfer from $Me_2Fc$ to $[(L_2)Co^{III}]$ to produce another $Me_2Fc^+$. In such a case, the rate of the formation of $Me_2Fc^+$ is given by Equation (16).

$$d[Me_2Fc^+]/dt = 2(k_{ET2} + k_{et2}[Me_2Fc])[Co_2^{III}(H_2O_2^{\bullet+})] \quad (16)$$

$$d[Co_2^{III}(H_2O_2^{\bullet+})]/dt = k_2[Co_2^{II}][O_2][H^+]^2 - (k_{-2} + k_{ET2} + k_{et2}[Me_2Fc])[Co_2^{III}(H_2O_2^{\bullet+})] \quad (17)$$

Under steady-state conditions ($d[Co_2^{III}(H_2O_2^{\bullet+})]/dt = 0$) in Equation (17), Equation (18) is obtained, which is reduced to Equation (19) under the conditions such that $k_{-2} \gg k_{ET2} + k_{et2}[Me_2Fc]$. Because $[(L_2)Co^{II}]$ remains constant during the catalytic reaction, Equation (19) is rewritten by Equation (20) (see Supporting Information for the derivation),

$$[Co_2^{III}(H_2O_2^{\bullet+})] = k_2[Co_2^{II}][O_2][H^+]^2/(k_{-2} + k_{ET2} + k_{et2}[Me_2Fc]) \quad (18)$$

$$[Co_2^{III}(H_2O_2^{\bullet+})] = K_2[Co_2^{II}][O_2][H^+]^2 \quad (19)$$

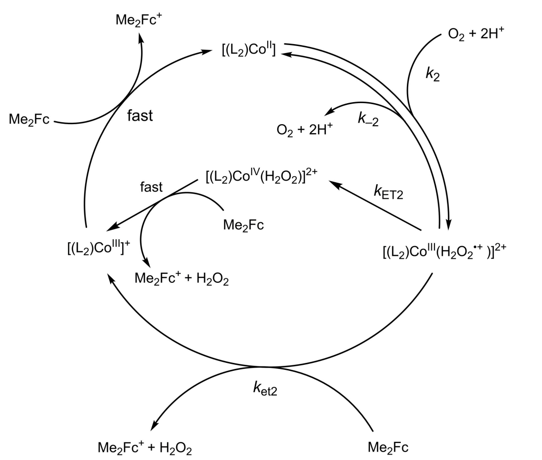


***Scheme 4.*** Proposed mechanism of catalytic two-electron/two-proton reduction of $O_2$ by $Me_2Fc$ with $[(L_2)Co^{II}]$ in the presence of HOTf.

$$[Co_2^{III}(H_2O_2^{\bullet+})] = K_2[Co_2^{II}]_0[O_2][H^+]^2/(1 + K_2[O_2][H^+]^2) \quad (20)$$

where $[Co_2^{II}]_0$ is the initial concentration of $[(L_2)Co^{II}]$. From Equations (16) and (20), Equation (21) is obtained under the conditions such that $k_{ET2} \ll k_{et2}[Me_2Fc]$. Thus, the dependence of $k_{cat2}$ on $[H^+]$ is given by Equation (22), which is the same as that of $k_{obs2}$ on [HOTf] and $[O_2]$ [Eq. (13)] when $k_{ET2}$ is replaced by $k_{et2}$. In this case, $k_{cat1}$ and $[(L_1)Co^{II}]$ are replaced by $k_{cat2}$ and $[(L_2)Co^{II}]$ in Equation (15). Equation (22) is rewritten by Equation (23).

$$d[Me_2Fc^+]/dt = \frac{2k_{et2}[Me_2Fc]K_2[Co_2^{II}]_0[O_2][H^+]^2}{(1 + K_2[O_2][H^+]^2)} \quad (21)$$

$$k_{cat2} = 2k_{et2}K_2[O_2][H^+]^2/(1 + K_2[O_2][H^+]^2) \quad (22)$$

$$(k_{cat2})^{-1} = (2k_{et2}K_2[O_2][H^+])^{-1} + (2k_{et2})^{-1} \quad (23)$$

A linear plot between $(k_{cat2})^{-1}$ vs $[HOTf]^{-2}$ is obtained as shown in Figure S37. From the intercept and slope, the $2k_{et2}$ and $K_2$ values were determined to be $(3.0 \pm 0.4) \times 10^{-2}\ s^{-1}$ and $(1.2 \pm 0.3) \times 10^4\ M^{-2}$, respectively. The $K_2$ value agrees within the experimental error with the value obtained from PCET from $[(L_2)Co^{II}]$ to $O_2$ $(1.8 \pm 0.4) \times 10^4\ M^{-2}$. Such an agreement indicates that the binding of two HOTf molecules to $[(L_2)Co^{III}(O_2^{\bullet-})]$ is involved in the r.d.s. in the catalytic two-electron reduction of $O_2$ by $Me_2Fc$ in the presence of HOTf in MeCN. The $k_{et2}$ value is much larger than the $k_2$ value because $k_{et2}$ is the rate constant of electron transfer from $Me_2Fc$ to $[(L_2)Co^{III}(H_2O_2^{\bullet+})]^{2+}$, which is much larger than that of the intramolecular electron transfer from the $Co^{III}$ moiety to the $H_2O_2^{\bullet+}$ moiety of $[(L_2)Co^{III}(H_2O_2^{\bullet+})]^{2+}$.

In the case of $[(L_1)Co^{II}]$, the $k_{cat1}$ values of the catalytic reduction of $O_2$ by $Me_2Fc$ with HOTf are larger than the $k_{cat2}$ values of $[(L_2)Co^{II}]$ in the HOTf concentration range up to 10 mM, because the protonation of the pendant imidazole ligand of $[(L_1)Co^{II}]$ facilitates the PCET reduction of $O_2$ to produce $[(L_1)Co^{III}(O_2H)]^+$, whereas the PCET reduction of $O_2$ by $[(L_2)Co^{II}]$ requires two protons and the first protonation equilibrium of $[(L_2)Co^{III}(O_2^{\bullet-})]$ is much smaller than the case of $[(L_1)Co^{III}(O_2^{\bullet-})]$ with the protonated pendant imidazole ligand. The dependence of the catalytic rate constants of two-electron/two-proton reduction of $O_2$ by $Me_2Fc$ on the acid concentration shows contrasting results: one is a saturated dependence for $[(L_1)Co^{II}]$ with a pendant imidazole ligand and the other is a sigmoidal dependence without a pendant imidazole ligand.

## *Conclusion*

We have demonstrated in this study that a pendant imidazole ligand attached to a cobalt(II) porphyrin, $[(L_1)Co^{II}]$, accelerates $O_2$ binding to produce a cobalt(III)-superoxide complex, $[(L_1)Co^{III}(O_2^{\bullet-})]$, due to the electron pushing effect of the axial imidazole ligand to the $Co^{II}$ center, as compared with a cobalt(II) porphyrin without the axial imidazole ligand, $[(L_2)Co^{II}]$. In the presence of HOTf, two-electron/two-proton reduction of $O_2$ by $Me_2Fc$ is catalyzed by both $[(L_1)Co^{II}]$ and $[(L_2)Co^{II}]$. The catalytic activity of $[(L_1)Co^{II}]$ is much higher than that of $[(L_2)Co^{II}]$, since the protonation of the pendant base in $[(L_1)Co^{II}]$ facilitates the PCET reduction of $O_2$, as compared with that of $[(L_2)Co^{II}]$ without the pendant base. The dependence of the catalytic rate constants of two-electron/two-proton reduction of $O_2$ by $Me_2Fc$ on the acid concentration shows contrasting results: one is a saturated dependence for $(L_1)Co^{II}]$ with a pendant imidazole ligand and the other is a sigmoidal dependence without a pendant imidazole ligand. Such crucial roles of the pendant base in both the stoichiometric and catalytic reduction of $O_2$, which have been clarified for the first time, provide valuable guide in developing more efficient catalysts for ORR. For example, introduction of electron-withdrawing groups in the amidophenyl (in $L_1$) group may facilitate the ORR reactivity.[32]

## Acknowledgements

This work was supported by the NRF of Korea (NRF-2021R1A3B1076539 to W.N and NRF-2020R1I1A1A01074630 to Y.-M.L.), the National Natural Science Foundation of China (21773146 and 22171176), Fok Ying-Tong Education Foundation for Outstanding Young Teachers in University, Fundamental Research Funds for the Central Universities, Research Funds of Shaanxi Normal University to R.C., and the National Natural Science Foundation of China (22102092) and the China Postdoctoral Science Foundation (2019M663614) to X.L.

## Conflict of Interest

The authors declare no conflict of interest.

## Data Availability Statement

The data that support the findings of this study are available in the Supporting Information of this article.

**Keywords:** Acid-Promoted Electron Transfer · Cobalt Porphyrin Complex · Pendant Imidazole Base · Reaction Mechanisms · Reduction of Dioxygen

[1] a) X. Li, H. Lei, L. Xie, N. Wang, W. Zhang, R. Cao, *Acc. Chem. Res.* **2022**, *55*, 878–892; b) X. Li, X.-P. Zhang, M. Guo, B. Lv, K. Guo, X. Jin, W. Zhang, Y.-M. Lee, S. Fukuzumi, W. Nam, R. Cao, *J. Am. Chem. Soc.* **2021**, *143*, 14613–14621; c) S. Zaman, L. Huang, A. I. Douka, H. Yang, R. You, B. Y. Xia, *Angew. Chem. Int. Ed.* **2021**, *60*, 17832–17852; *Angew. Chem.* **2021**, *133*, 17976–17996; d) C.-X. Zhao, J.-N. Liu, J. Wang, D. Ren, B.-Q. Li, Q. Zhang, *Chem. Soc. Rev.* **2021**, *50*, 7745–7778.

[2] a) M. Mukherjee, A. Dey, *JACS Au* **2021**, *1*, 1296–1311; b) M. L. Pegis, C. F. Wise, D. J. Martin, J. M. Mayer, *Chem. Rev.* **2018**, *118*, 2340–2391; c) M. Wikström, K. Krab, V. Sharma, *Chem. Rev.* **2018**, *118*, 2469–2490.

[3] a) D. J. Martin, C. F. Wise, M. L. Pegis, J. M. Mayer, *Acc. Chem. Res.* **2020**, *53*, 1056–1065; b) W. Zhang, W. Lai, R. Cao, *Chem. Rev.* **2017**, *117*, 3717–3797.

[4] a) X. F. Lu, B. Y. Xia, S.-Q. Zang, X. W. Lou, *Angew. Chem. Int. Ed.* **2020**, *59*, 4634–4650; *Angew. Chem.* **2020**, *132*, 4662–4678; b) A. A. Gewirth, J. A. Varnell, A. M. DiAscro, *Chem. Rev.* **2018**, *118*, 2313–2339.

[5] a) H. Lei, X. Li, J. Meng, H. Zheng, W. Zhang, R. Cao, *ACS Catal.* **2019**, *9*, 4320–4344; b) S. Fukuzumi, Y.-M. Lee, W. Nam, *Chem. Eur. J.* **2018**, *24*, 5016–5031; c) S. Fukuzumi, *Joule* **2017**, *1*, 689–738.

[6] a) E. Miglbauer, M. Gryszel, E. D. Głowacki, *Green Chem.* **2020**, *22*, 673–677; b) S. Fukuzumi, Y. Yamada, *ChemElectroChem* **2016**, *3*, 1978–1989.

[7] a) Q. Wu, J. Cao, X. Wang, Y. Liu, Y. Zhao, H. Wang, Y. Liu, H. Huang, F. Liao, M. Shao, Z. Kang, *Nat. Commun.* **2021**, *12*, 483; b) Y. Shiraishi, T. Takii, T. Hagi, S. Mori, Y. Kofuji, Y. Kitagawa, S. Tanaka, S. Ichikawa, T. Hirai, *Nat. Mater.* **2019**, *18*, 985–993.

[8] a) K. Mase, M. Yoneda, Y. Yamada, S. Fukuzumi, *ACS Energy Lett.* **2016**, *1*, 913–919; b) K. Mase, M. Yoneda, Y. Yamada, S. Fukuzumi, *Nat. Commun.* **2016**, *7*, 11470.

[9] a) J. Tian, D. Wang, S. Li, Y. Pei, M. Qiao, Z.-H. Li, J. Zhang, B. Zong, *ACS Sustain. Chem. Eng.* **2020**, *8*, 594–603; b) C. Zhu, M. Zhu, Y. Sun, Y. Zhou, J. Gao, H. Huang, Y. Liu, Z. Kang, *ACS Appl. Energy Mater.* **2019**, *2*, 8737–8746.

[10] a) C. W. Machan, *ACS Catal.* **2020**, *10*, 2640–2655; b) Y. Yang, R. Zeng, Y. Xiong, F. J. DiSalvo, H. D. Abruña, *J. Am. Chem. Soc.* **2019**, *141*, 19241–19245; c) C. Gu, X. Nie, J. Jiang, Z. Chen, Y. Dong, X. Zhang, J. Liu, Z. Yu, Z. Zhu, J. Liu, X. Liu, Y. Shao, *J. Am. Chem. Soc.* **2019**, *141*, 13212–13221; d) C. W. Anson, S. S. Stahl, *J. Am. Chem. Soc.* **2017**, *139*, 18472–18475.

[11] a) R. Zhang, J. J. Warren, *J. Am. Chem. Soc.* **2020**, *142*, 13426–13434; b) P. Peljo, L. Murtomäki, T. Kallio, H. J. Xu, M. Meyer, C. P. Gros, J. M. Barbe, H. H. Girault, K. Laasonen, K. Kontturi, *J. Am. Chem. Soc.* **2012**, *134*, 5974–5984; c) B. Su, I. Hatay, A. Trojánek, Z. Samec, T. Khoury, C. P. Gros, J. M. Barbe, A. Daina, P. A. Carrupt, H. H. Girault, *J. Am. Chem. Soc.* **2010**, *132*, 2655–2662; d) S. Fukuzumi, K. Okamoto, C. P. Gros, R. Guilard, *J. Am. Chem. Soc.* **2004**, *126*, 10441–10449.

[12] a) A. W. Nichols, E. N. Cook, Y. J. Gan, P. R. Miedaner, J. M. Dressel, D. A. Dickie, H. S. Shafaat, C. W. Machan, *J. Am. Chem. Soc.* **2021**, *143*, 13065–13073; b) Y. Liu, G. Zhou, Z. Zhang, H. Lei, Z. Yao, J. Li, J. Lin, R. Cao, *Chem. Sci.* **2020**, *11*, 87–96; c) Y. Sun, L. Silvioli, N. R. Sahraie, W. Ju, J. Li, A. Zitolo, S. Li, A. Bagger, L. Arnarson, X. Wang, T. Moeller, D. Bernsmeier, J. Rossmeisl, F. Jaouen, P. Strasser, *J. Am. Chem. Soc.* **2019**, *141*, 12372–12381; d) Y. H. Wang, P. E. Schneider, Z. K. Goldsmith, B. Mondal, S. Hammes-Schiffer, S. S. Stahl, *ACS Cent. Sci.* **2019**, *5*, 1024–1034.

[13] a) H. Lei, C. Liu, Z. Wang, Z. Zhang, M. Zhang, X. Chang, W. Zhang, R. Cao, *ACS Catal.* **2016**, *6*, 6429–6437; b) G. Passard, A. M. Ullman, C. N. Brodsky, D. G. Nocera, *J. Am. Chem. Soc.* **2016**, *138*, 2925–2928; c) K. Mase, K. Ohkubo, S. Fukuzumi, *Inorg. Chem.* **2015**, *54*, 1808–1815.

[14] a) A. C. Brezny, S. I. Johnson, S. Raugei, J. M. Mayer, *J. Am. Chem. Soc.* **2020**, *142*, 4108–4113; b) A. Ghatak, S. Bhakta, S. Bhunia, A. Dey, *Chem. Sci.* **2019**, *10*, 9692–9698; c) S. L. Hooe, C. W. Machan, *J. Am. Chem. Soc.* **2019**, *141*, 4379–4387; d) L. Wang, M. Gennari, F. G. Cantú Reinhard, J. Gutiérrez, A. Morozan, C. Philouze, S. Demeshko, V. Artero, F. Meyer, S. P. de Visser, C. Duboc, *J. Am. Chem. Soc.* **2019**, *141*, 8244–8253;

e) Z. Halime, H. Kotani, Y. Li, S. Fukuzumi, K. D. Karlin, *Proc. Natl. Acad. Sci. USA* **2011**, *108*, 13990–13994.

[15] a) H. Oh, S. Choi, J. Y. Kim, H. S. Ahn, S. Hong, *Chem. Commun.* **2019**, *55*, 12659–12662; b) S. Kakuda, C. J. Rolle, K. Ohkubo, M. A. Siegler, K. D. Karlin, S. Fukuzumi, *J. Am. Chem. Soc.* **2015**, *137*, 3330–3337; c) S. Kakuda, R. L. Peterson, K. Ohkubo, K. D. Karlin, S. Fukuzumi, *J. Am. Chem. Soc.* **2013**, *135*, 6513–6522.

[16] a) Y. Zhao, P. Zhang, Z. Yang, L. Li, J. Gao, S. Chen, T. Xie, C. Diao, S. Xi, B. Xiao, C. Hu, W. Choi, *Nat. Commun.* **2021**, *12*, 3701; b) H. W. Kim, V. J. Bukas, H. Park, S. Park, K. M. Diederichsen, J. Lim, Y. H. Cho, J. Kim, W. Kim, T. H. Han, J. Voss, A. C. Luntz, B. D. McCloskey, *ACS Catal.* **2020**, *10*, 852–863; c) W. Suzuki, H. Kotani, T. Ishizuka, T. Kojima, *J. Am. Chem. Soc.* **2019**, *141*, 5987–5994.

[17] a) H. Zhang, Y. Zhao, Y. Li, G. Li, J. Li, F. Zhang, *ACS Appl. Energy Mater.* **2020**, *3*, 705–714; b) Z. Lu, G. Chen, S. Siahrostami, Z. Chen, K. Liu, J. Xie, L. Liao, T. Wu, D. Lin, Y. Liu, T. F. Jaramillo, J. K. Nørskov, Y. Cui, *Nat. Catal.* **2018**, *1*, 156–162.

[18] a) G. Passard, D. K. Dogutan, M. Qiu, C. Costentin, D. G. Nocera, *ACS Catal.* **2018**, *8*, 8671–8679; b) M. Guo, Y.-M. Lee, R. Gupta, M. S. Seo, T. Ohta, H.-H. Wang, H.-Y. Liu, S. N. Dhuri, R. Sarangi, S. Fukuzumi, W. Nam, *J. Am. Chem. Soc.* **2017**, *139*, 15858–15867.

[19] a) E. N. Cook, D. A. Dickie, C. W. Machan, *J. Am. Chem. Soc.* **2021**, *143*, 16411–16418; b) L. Xie, X.-P. Zhang, B. Zhao, P. Li, J. Qi, X. Guo, B. Wang, H. Lei, W. Zhang, U.-P. Apfel, R. Cao, *Angew. Chem. Int. Ed.* **2021**, *60*, 7576–7581; *Angew. Chem.* **2021**, *133*, 7654–7659; c) M. L. Pegis, D. J. Martin, C. F. Wise, A. C. Brezny, S. I. Johnson, L. E. Johnson, N. Kumar, S. Raugei, J. M. Mayer, *J. Am. Chem. Soc.* **2019**, *141*, 8315–8326; d) M. Okamura, M. Kondo, R. Kuga, Y. Kurashige, T. Yanai, S. Hayami, V. K. K. Praneeth, M. Yoshida, K. Yoneda, S. Kawata, S. Masaoka, *Nature* **2016**, *530*, 465–468.

[20] a) A. Rana, Y.-M. Lee, X. Li, R. Cao, S. Fukuzumi, W. Nam, *ACS Catal.* **2021**, *11*, 3073–3083; b) B. Lv, X. Li, K. Guo, J. Ma, Y. Wang, H. Lei, F. Wang, X. Jin, Q. Zhang, W. Zhang, R. Long, Y. Xiong, U.-P. Apfel, R. Cao, *Angew. Chem. Int. Ed.* **2021**, *60*, 12742–12746; *Angew. Chem.* **2021**, *133*, 12852–12856; c) B. Mondal, S. Chattopadhyay, S. Dey, A. Mahammed, K. Mittra, A. Rana, Z. Gross, A. Dey, *J. Am. Chem. Soc.* **2020**, *142*, 21040–21049.

[21] C. Kuai, C. Xi, A. Hu, Y. Zhang, Z. Xu, D. Nordlund, C.-J. Sun, C. A. Cadigan, R. M. Richards, L. Li, C.-K. Dong, X.-W. Du, F. Lin, *J. Am. Chem. Soc.* **2021**, *143*, 18519–18526.

[22] a) A. Ali, D. Prakash, P. Majumder, S. Ghosh, A. Dutta, *ACS Catal.* **2021**, *11*, 5934–5941; b) Y. Liu, Y. Han, Z. Zhang, W. Zhang, W. Lai, Y. Wang, R. Cao, *Chem. Sci.* **2019**, *10*, 2613–2622; c) M. Langerman, D. G. H. Hetterscheid, *Angew. Chem. Int. Ed.* **2019**, *58*, 12974–12978; *Angew. Chem.* **2019**, *131*, 13108–13112; d) N. Thiyagarajan, D. Janmanchi, Y.-F. Tsai, W. H. Wanna, R. Ramu, S. I. Chan, J.-M. Zen, S. S.-F. Yu, *Angew. Chem. Int. Ed.* **2018**, *57*, 3612–3616; *Angew. Chem.* **2018**, *130*, 3674–3678; e) P. Garrido-Barros, I. Funes-Ardoiz, S. Drouet, J. Benet-Buchholz, F. Maseras, A. Llobet, *J. Am. Chem. Soc.* **2015**, *137*, 6758–6761.

[23] S. M. Adam, G. B. Wijeratne, P. J. Rogler, D. E. Diaz, D. A. Quist, J. J. Liu, K. D. Karlin, *Chem. Rev.* **2018**, *118*, 10840–11022.

[24] a) M. Lancaster, P. Moënne-Loccoz, D. P. Goldberg, *J. Am. Chem. Soc.* **2019**, *141*, 3641–3653; b) D. A. Quist, M. A. Ehudin, A. W. Schaefer, G. L. Schneider, E. I. Solomon, K. D. Karlin, *J. Am. Chem. Soc.* **2019**, *141*, 12682–12696; c) N. Kindermann, C. J. Günes, S. Dechert, F. Meyer, *J. Am. Chem. Soc.* **2017**, *139*, 9831–9834.

[25] a) X.-Y. Zhou, C. Xu, P.-P. Guo, W.-L. Sun, P.-J. Wei, J.-G. Liu, *Chem. Eur. J.* **2021**, *27*, 9898–9904; b) J. Chlistunoff, J.-M. Sansiñena, *J. Phys. Chem. C* **2014**, *118*, 19139–19149; c) M. Tsuda, H. Kasai, *Surf. Sci.* **2007**, *601*, 5200–5206.

[26] The formal $Co^{I/0}$ couple at $-2.10$ V is quite reversible, probably, because of the one-electron reduction of the porphyrin ligand instead of $Co^{I/0}$ couple. However, the exact assignment of this redox event, which is not the interest of this work, has yet to be confirmed, but such a discussion on CV will not affect the conclusion made in this work.

[27] J. P. Collman, Y.-L. Yan, T. Eberspacher, X. Xie, E. I. Solomon, *Inorg. Chem.* **2005**, *44*, 9628–9630.

[28] D. Sazou, C. Araullo-McAdams, B. C. Han, M. M. Franzen, K. M. Kadish, *J. Am. Chem. Soc.* **1990**, *112*, 7879–7886.

[29] a) R. D. Jones, D. A. Summerville, F. Basolo, *Chem. Rev.* **1979**, *79*, 139–179; b) F. A. Walker, *J. Am. Chem. Soc.* **1970**, *92*, 4235–4244.

[30] a) S. Fukuzumi, K.-B. Cho, Y.-M. Lee, S. Hong, W. Nam, *Chem. Soc. Rev.* **2020**, *49*, 8988–9027; b) S. Fukuzumi, Y.-M. Lee, W. Nam, *Bull. Korean Chem. Soc.* **2020**, *41*, 1217–1232; c) S. Fukuzumi, Y.-M. Lee, W. Nam, *Bull. Korean Chem. Soc.* **2021**, *42*, 1558–1568.

[31] a) T. Devi, Y.-M. Lee, W. Nam, S. Fukuzumi, *Coord. Chem. Rev.* **2020**, *410*, 213219; b) T. Devi, Y.-M. Lee, W. Nam, S. Fukuzumi, *J. Am. Chem. Soc.* **2020**, *142*, 365–372.

[32] S. Fukuzumi, K. Ohkubo, *Chem. Eur. J.* **2000**, *6*, 4532–4535.

[33] S. Fukuzumi, S. Kuroda, T. Tanaka, *J. Am. Chem. Soc.* **1985**, *107*, 3020–3027.

Manuscript received: June 2, 2022
Accepted manuscript online: June 21, 2022
Version of record online: July 13, 2022